The properties of isolated chiral skyrmions in thin magnetic films

Leonov, A. O.; Monchesky, T. L.; Romming, N.; Kubetzka, A.; Bogdanov, A. N.; Wiesendanger, R.

Published in:
New Journal of Physics

DOI:
10.1088/1367-2630/18/6/065003

Publication date:
2016

New Journal of Physics
The open access journal at the forefront of physics

Deutsche Physikalische Gesellschaft DPG IOP Institute of Physics

PAPER • OPEN ACCESS

The properties of isolated chiral skyrmions in thin magnetic films

To cite this article: A O Leonov *et al* 2016 *New J. Phys.* **18** 065003

New Journal of Physics
The open access journal at the forefront of physics

Deutsche Physikalische Gesellschaft DPG
IOP Institute of Physics

Published in partnership with: Deutsche Physikalische Gesellschaft and the Institute of Physics

OPEN ACCESS

RECEIVED
29 February 2016

REVISED
14 April 2016

ACCEPTED FOR PUBLICATION
5 May 2016

PUBLISHED
31 May 2016

PAPER

The properties of isolated chiral skyrmions in thin magnetic films

A O Leonov[1,2,5], T L Monchesky[3], N Romming[4], A Kubetzka[4], A N Bogdanov[1] and R Wiesendanger[4]

[1] IFW Dresden, Postfach 270016, D-01171 Dresden, Germany
[2] Zernike Institute for Advanced Materials, University of Groningen, Groningen, 9700AB, The Netherlands
[3] Department of Physics and Atmospheric Science, Dalhousie University, Halifax, Nova Scotia, Canada B3H 3J5
[4] Department of Physics, University of Hamburg, D-20355 Hamburg, Germany
[5] Author to whom any correspondence is addressed.

E-mail: a.leonov@rug.nl

Keywords: chiral skyrmion, collapse field, thin films

Abstract

Axisymmetric solitonic states (*chiral skyrmions*) were first predicted theoretically more than two decades ago. However, until recently they have been observed in a form of skyrmionic condensates (hexagonal lattices and other mesophases). In this paper we report experimental and theoretical investigations of *isolated* chiral skyrmions discovered in PdFe/Ir(111) bilayers two years ago by Romming *et al* (2013 *Science* **341** 636). The results of spin-polarized scanning tunneling microscopy analyzed within the continuum and discrete models provide a consistent description of isolated skyrmions in thin layers. The existence region of chiral skyrmions is restricted by strip-out instabilities at low fields and a collapse at high fields. We demonstrate that the same equations describe axisymmetric localized states in all condensed matter systems with broken mirror symmetry, and thus our findings establish basic properties of isolated skyrmions common for chiral liquid crystals, different classes of noncentrosymmetric magnets, ferroelectrics, and multiferroics.

1. Introduction

Long-period homochiral magnetization modulations (*helical* phases) [1] and axisymmetric solitonic patterns (*vortices* or *skyrmions*) [2–4] are two types of unconventional magnetic states attributed solely to magnetic compounds with broken inversion symmetry and distinguish them from common (achiral) magnetic materials (figures 1, 2). Both, extended chiral modulated phases and localized skyrmionic states are stabilized by specific *Dzyaloshinskii-Moriya* (DM) interactions arising in chiral magnets owing to their crystallographic handedness [1]. In the micromagnetic energy functionals of noncentrosymmetric ferromagnets these interactions are described by energy contributions linear in the first spatial derivatives of the magnetization **M** (*Lifshitz* invariants) [1]

$$M_i \frac{\partial M_j}{\partial x_k} - M_j \frac{\partial M_i}{\partial x_k}. \quad (1)$$

Axisymmetric localized structures (figure 1) are related to multidimensional topological solitons with nonsingular internal structure and finite energy [5]. These particle-like objects are of special interest in fundamental physics and mathematics [6–8]. In most nonlinear physical systems, multidimensional solitons can exist only as dynamic excitations [9]. However, the corresponding static solutions are unstable and collapse spontaneously into topological singularities [10].

In nonlinear field theory, the existence and stability of skyrmion solutions is provided by special terms in the energy functionals. More than five decades ago T H Skyrme introduced into the nonlinear field model an interaction term with higher order spatial derivatives that stabilize two- and three-dimensional topological nonsingular solitons (now commonly addressed as *skyrmions*) [11]. Since that time, field theorists have been intensively investigating this family of solitons (skyrmions) within the Faddeev–Skyrme and kindred models [6, 11, 12].

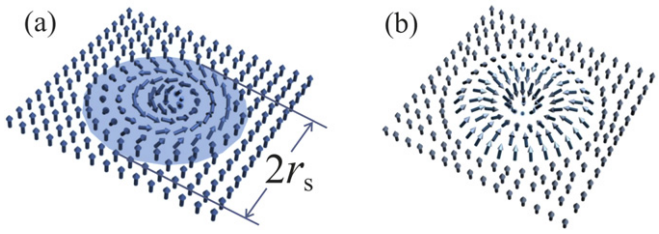

Figure 1. Axisymmetric isolated skyrmions: (a) in cubic helimagnets and uniaxial ferromagnets with D_n symmetry; (b) in uniaxial ferromagnets with C_{nv} symmetry [2].

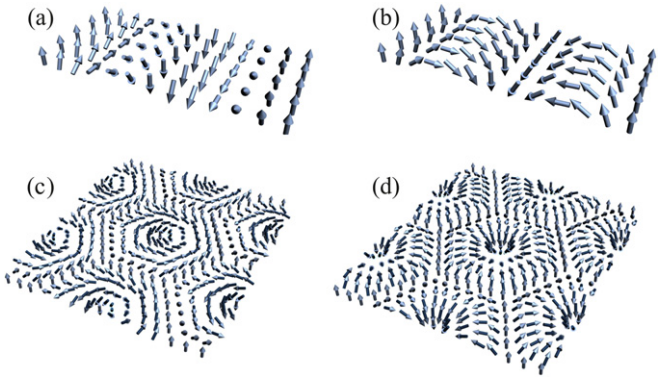

Figure 2. Basic modulated phases in chiral ferromagnets: one-dimensional *helicoids* (a) and *cycloids* (b) and two-dimensional *skyrmion lattices* (c, d). Bloch-type modulations (a, c) arise in cubic helimagnets and ferromagnets with D_n symmetries; Néel-type modulations (b, d) are attributed to uniaxial ferromagnets with C_{nv} symmetries [2].

Lifshitz invariants of type (1) provide the only known alternative to the Skyrme mechanism that yield regular solutions for axisymmetric skyrmions [3, 13–15]. These invariants arising in noncentrosymmetric condensed matter systems (including chiral magnets, liquid crystals, multiferroics, and nanolayers of magnetic metals with interface induced Dzyaloshinskii–Moriya interactions) introduce a unique class of materials where mesoscopic skyrmions can be induced and manipulated.

In a broad range of applied magnetic fields and temperatures isolated skyrmions condense into hexagonal lattices [3, 16, 17] or other types of two-dimensional modulated states [18, 19]. During the last years, intensive experimental efforts have been undertaken to find indications of hexagonal skyrmion lattices in different groups of chiral ferromagnets (see e.g [20–29] and bibliography in [17]). Particularly, direct observations of skyrmion lattices have been reported in free standing nanolayers of cubic helimagnets in [23] (and the following papers of this group [24, 30]). These results reveal axial symmetry and homochirality of the embedded skyrmions, and observed properties of skyrmion lattices were found to be in close correspondence with theoretical results. To date the LTEM studies of confined cubic helimagnets have focused on the skyrmion condensates (skyrmion lattices and clusters) [23, 24, 29, 30]. Spin-polarized scanning tunneling microscopy (SP-STM) has been able to identify isolated skyrmions in the saturated states of PdFe/Ir(111) films [31], and subsequently resolve their internal structure [32].

From a theoretical perspective, the basic magnetic properties of isolated skyrmions and skyrmion lattices in bulk noncentrosymmetric magnets have been investigated in a number of earlier contributions [3, 14, 33]. Recently the experimental advances in the observation of chiral skyrmion states [16, 18, 21–30] have renewed the interest to this phenomenon and triggered intensive theoretical studies of stationary and moving skyrmions [17, 19, 35–37, 42–47, 49–51]. In most of these contributions, only magnetic properties of bound skyrmionic states are addressed (skyrmion lattices and individual skyrmions confined in nanodots, narrow strips, nanowires). However, modern theoretical studies have practically paid no attention to the properties of isolated skyrmions, which are fundamental to understanding the physics of magnetic skyrmions and their applications in potential spintronic devices [34, 46].

The discoveries of isolated chiral skyrmions in PdFe/Ir (111) bilayers [31] and the method for a determination of their internal structure [32] open up a new dimension in the investigations of chiral skyrmions.

Our paper devoted to experimental and theoretical investigations of the evolution of isolated skyrmion structures under the influence of applied magnetic fields represent the first step in this direction.

In the theoretical part of this paper (section 2) we develop the first consistent theory of isolated chiral skyrmions in thin magnetic layers and apply our findings for the analysis of isolated skyrmions observed in PdFe/Ir(111) bilayers. In section 2.2 we apply the qualitative theory of differential equations to expound main features of isolated chiral skyrmions and elucidate their physical nature, investigate the conditions of the elliptical instability at low fields and calculate within the discrete model the skyrmion collapse field. In section IIC we construct the phase diagram of the solutions for isolated skyrmions.

In the experimental part we present the detailed evolution of isolated skyrmions in PdFe/Ir(111) bilayers from the strip-out at low fields to the collapse at high fields.

2. Theory

A phenomenological theory of chiral modulations in noncentrosymmetric magnetic crystals has been developed by I. Dzyaloshinskii in 1964 [1]. These papers also include analytical solutions for one-dimensional chiral modulations (*helicoids* and *cycloids*). Theoretical investigations of chiral modulations in bulk and confined noncentrosymmetric ferro- and antiferromagnets have been carried out in many of the papers discussed in [17].

2.1. The micromagnetics of chiral modulations

2.1.1. Energy functional and symmetry

In this paper we investigate isolated skyrmions in a thin layer of a noncentrosymmetric ferromagnet. As a model we consider a thin plate infinite along the $x-$ and $y-$ axes and of thickness L along the $z-$ axis. In the following sections we specify the model and discuss its limitations. For a film of a noncentrosymmetric uniaxial ferromagnet in the applied magnetic field $\mathbf{H}^{(e)}$ perpendicular to the film surface, the micromagnetic energy density written within terms quadratic in the components of the magnetization vector $\mathbf{M}$ has the following standard form [1]:

$$w = A\,(\mathbf{grad}\ \mathbf{m})^2 + w_D(\mathbf{m}) - K\,(\mathbf{m}\cdot\mathbf{n})^2 - \mu_0 M H^{(e)}\mathbf{m}\cdot\mathbf{n} - \mu_0 M\mathbf{m}\cdot\mathbf{H}^{(d)}/2, \tag{2}$$

where A is the exchange stiffness constant, K is the uniaxial anisotropy constant, $\mathbf{H}^{(d)}$ is the demagnetizing field,

$$\mathbf{m} = \mathbf{M}/|\mathbf{M}| = (\sin\theta\cos\psi,\ \sin\theta\sin\psi,\ \cos\theta) \tag{3}$$

is the reduced magnetization, $\mathbf{n}$ is the unity vector directed perpendicular to the film surface.

The Dzyaloshinskii-Moriya energy density w_D is composed of Lifshitz invariants (1):

$$\mathcal{L}_{ij}^{(k)} = m_i\frac{\partial m_j}{\partial x_k} - m_j\frac{\partial m_i}{\partial x_k}. \tag{4}$$

The functional forms of energy density w_D are determined by crystallographic symmetry of a noncentrosymmetric magnetic crystal and are listed in equations (A.1), (A.2). Lifshitz invariants (4) favour spatial modulations with a fixed rotation sense along the x_k directions [1]. A competition between the chiral energy w_D and other energy contributions leads to the formation of isolated chiral states [2, 3, 14] and spatially modulated magnetic phases [1, 3].

The Euler equations for energy functional (2) together with Maxwell's equations,

$$\mathrm{rot}\mathbf{H}^{(d)} = 0, \quad \mathrm{div}\,[\mathbf{H}^{(d)} + \mu_0\mathbf{M}] = 0, \tag{5}$$

yield solutions for different types of chiral modulations (figures 1, 2, 12).

2.1.2. Demagnetization effects

Generally the equilibrium modulated patterns $\mathbf{m}(\mathbf{r})$ in a chiral magnet are derived by numerically solving the above set of nonlinear differential equations including non-local stray-field calculations [14, 34]. Contrary to soft magnetic materials where demagnetization fields sufficiently influence the equilibrium magnetic states [38], in chiral magnetic materials the DM interactions strongly suppress these effects [34]. As a result in many practical cases a magnetostatic problem is reduced to analytical solutions [3, 34, 39], and the stray-field energy can be expressed as local energy contributions in energy functional (2) [3, 34].

It was also found that for one-dimensional modulations and two-dimensional axisymmetric structures, the internal stray-field energy has a local character [3, 38]. Particularly, for ferromagnets with C_{nv} symmetry the internal stray-field energy can be taken into account by the following redefinition of the anisotropy constant,

$$K \to K + K_d, \quad K_d = \mu_0 M^2/2. \tag{6}$$

2.1.3. The equations for axisymmetic skyrmions

We introduce cylindrical coordinates for the spatial variable $\mathbf{r} = (r\cos\varphi,\ r\sin\varphi,\ z)$ and consider magnetic patterns homogeneous along the z-axis with the magnetization antiparallel to the applied field in the center ($\theta = \pi$ for $r = 0$) and approaching the parallel orientation when the distance from the center approaches infinity ($\theta \to 0$ for $r \to \infty$). For $\theta(r,\ \varphi)$, $\psi(r,\ \varphi)$ the energy functional (2) is reduced to the following form:

$$w = A\left[\theta_r^2 + \frac{1}{r^2}\theta_\varphi^2 + \sin^2\theta\left(\psi_r^2 + \frac{1}{r^2}\psi_\varphi^2\right)\right] + w_D - K\cos^2\theta - \mu_0 M H^{(e)}\cos\theta - \mu_0 M\mathbf{m}\cdot\mathbf{H}^{(d)}/2, \quad (7)$$

and the Dzyaloshinskii-Moriya energy functionals $w_D(\theta,\ \psi,\ r,\ \varphi)$ are listed in equations (A.1), (A.2).

The equations minimizing energy (7) include rotationally symmetric solutions,

$$\theta = \theta(r), \quad \psi = \psi(\varphi), \quad \mathbf{H}^{(d)} = \mathbf{H}^{(d)}(r). \quad (8)$$

Analytical solutions $\psi = \psi(\varphi)$ for uniaxial noncentrosymmetric ferromagnets [2] and cubic helimagnets (figures 1, 2) are listed in equation (A.7).

To date, only two types of skyrmionic states from this list have been identified in chiral ferromagnets by direct experimental observations: skyrmionic patterns with Bloch-type modulations (figure 1(a))

$$\mathbf{m} = \vec{e}_\varphi \sin\theta(r) + \vec{e}_z\cos\theta(r) \quad (9)$$

have been observed in free standing nanolayers of cubic helimagnets (see e.g. [23, 24, 30]), and skyrmion lattices with Néel-type modulations (figure 1(b))

$$\mathbf{m} = \vec{e}_r \sin\theta(r) + \vec{e}_z\cos\theta(r) \quad (10)$$

have been observed in Fe/Ir(111) and PdFe/Ir(111) nanolayers [27, 31, 32, 41] and in the rhombohedral ferromagnet GaV_4O_8 with C_{3v} symmetry [28].

The first direct observations of isolated skyrmions have been reported in PdFe/Ir(111) nanolayers [31]. These chiral solitonic structures have been investigated in a broad range of applied fields [31, 32].

After integration with respect to ϕ, the total energy $\mathcal{F}$ for an isolated skyrmion of Bloch- and Néel-type in an applied magnetic field perpendicular to the film surface can be reduced to the following form:

$$\mathcal{F} = 2\pi\int_0^\infty f(\theta,\ r)r\mathrm{d}r. \quad (11)$$

Here $f(\theta,\ r) = w(\theta,\ r) - w(0)$ is the difference between the skyrmion energy density and that of the saturated state, $w(0) = -K - \mu_0 MH$:

$$f(\theta,\ r) = A\left(\theta_r^2 + \frac{1}{r^2}\sin^2\theta\right) - D\left(\theta_r + \frac{1}{r}\sin\theta\cos\theta\right) + K\sin^2\theta + \mu_0 H(1 - \cos\theta). \quad (12)$$

In equation (12) the perpendicular component of the internal magnetic field $H \equiv H_z$ equals the difference between the value of the applied magnetic field $H^{(e)} \equiv H_z^{(e)}$ and the perpendicular component of the demagnetization field imposed by the film with an isolated axisymmetric skyrmion ($H_d^{(\mathrm{sk})}$): $H = H^{(e)} - H_d^{(\mathrm{sk})}$. The analytical solution for the stray-field $H_d^{(\mathrm{sk})}$ has been derived by Y. Tu [34, 39]. In most nanolayers of chiral magnets investigated so far, skyrmion sizes are smaller than the layer thickness ($r_s < d$). For such 'thick' films the stray-field $H_d^{(\mathrm{sk})}$ can be simplified and yields the following relation between the applied and internal fields: $H = H^{(e)} - \mu_0 M$. In PdFe/Ir (111) films investigated in this paper, isolated skyrmion cores are much larger than the film thickness ($r_s \gg d$). In this limiting case of 'ultrathin' films, the stray-field $H_d^{(\mathrm{sk})}$ becomes exponentially small due to dipole-dipole interactions between the upper and bottom film surfaces, and the internal field is practically equal to the external field ($H \cong H^{(e)}$). A similar drastic reduction of the stray-field occurs in ultrathin magnetic films with isolated bubble and stripe domains [40].

The Euler equation for energy functional (12),

$$A\left(\theta_{rr} + \frac{1}{r}\theta_r - \frac{1}{r^2}\sin\theta\cos\theta\right) + \frac{D}{r}\sin^2\theta - K\sin\theta\cos\theta - \mu_0 MH\sin\theta = 0, \quad (13)$$

with boundary conditions

$$\theta(0) = \pi, \quad \theta(\infty) = 0, \quad (14)$$

yields the equilibrium structure of isolated axisymmetric skyrmions [2, 3, 14]. Note that for Néel-type skyrmions, K includes the stray energy contribution (6).

Dimensionless variables

$$\rho = 2\pi r/L_D, \quad h = H/H_D, \quad k = K/K_0, \quad (15)$$

are commonly used in recent papers to describe modulated states in uniaxial chiral ferromagnets and cubic helimagnets (see e.g. [17, 26, 32, 42]). Here we use the characteristic parameters of a uniaxial chiral ferromagnet [3, 42]:

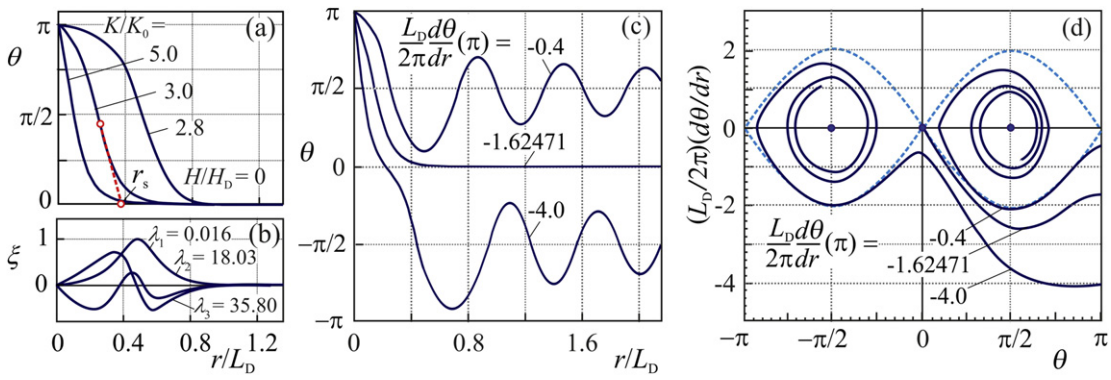

Figure 3. (a) Typical localized solutions of the boundary value problem with magnetization profile $\theta(\rho)$. The first three excitation modes $\xi_i(\rho)$ with positive eigenvalues λ_i (b) for the solution for $K/K_0 = 2.8$. 'Shooting trajectories $\theta(\rho)$ of the Cauchy problem (c) and corresponding phase trajectories $\theta_\rho(\theta)$ (d).

$$L_D = \frac{4\pi A}{|D|}, \quad \mu_0 H_D = \frac{D^2}{2AM}, \quad K_0 = \frac{D^2}{4A}. \tag{16}$$

L_D is the period of a helix at zero field and zero anisotropy, H_D is the saturated field and K_0 is the critical anisotropy (A.13).

With variables (15), the equation for axisymmetric skyrmions (13) is reduced to the following form:

$$\theta_{\rho\rho} + \frac{\theta_\rho}{\rho} - \frac{1}{\rho^2}\sin\theta\cos\theta + \frac{2\sin^2\theta}{\rho} - k\sin\theta\cos\theta - h\sin\theta = 0, \tag{17}$$

with boundary conditions (14).

2.2. Solutions for axisymmetric skyrmions

The equilibrium skyrmion profiles $\theta(\rho)$ are derived by solving the boundary value problem (13) and (14) with a finite-difference method [14]. Typical solutions of equation (13) are plotted in figure 3, and the existence areas for isolated skyrmions are indicated in the phase diagram of the solutions (figure 4).

The solutions $\theta(\rho)$ are linear near the skyrmion axis ($(\pi - \theta) \propto \rho$ for $\rho \ll 1$) and decay exponentially at high distances from the center ($\rho \gg 1$) $\theta \propto \exp(-\rho\sqrt{k+h})/\sqrt{\rho}$.

Usually the functions $\theta(\rho)$ have arrow-like shape with the steepest slope at the center of the skyrmion ($r = 0$). They transform into bell-shape profiles only near the critical line H_{el}. In micromagnetism, the characteristic size of a localized magnetization profile $\theta(\rho)$ is defined as [38]

$$r_s = r_0 - \theta_0\,(\mathrm{d}\theta/\mathrm{d}r)^{-1}_{r=r_0}, \tag{18}$$

where $(r_0,\ \theta_0)$ is the inflection point of the profile $\theta(r)$ (figure 3(a)).

Theoretically, chiral skyrmions have been investigated by numerical methods in many recent publications [17, 19, 35–37, 42–50]. These findings demonstrate their rich spectrum of magnetic states characteristic for chiral skyrmions and various scenarios of their evolution under the influence of applied fields [46, 49, 50]. However, they still require substantial analytical analysis and physical comprehension. The qualitative theory of nonlinear differential equations together with other analytical methods provide effective tools to gain important insight into the physics of chiral skyrmions and establish mathematical relations between them and other types of magnetic solitons.

2.2.1. Visualization of solutions on the $(\theta,\ \theta_r)$ phase plane

Solutions $\theta(r)$ of the boundary value problem (14) can be derived by solving the auxiliary Cauchy initial value problem for equation (13),

$$\theta(0) = \pi, \quad \theta_r(0) = -a. \tag{19}$$

For illustration we consider the Cauchy problem given by (13) and (19) for $H = 0$ and $\varkappa = \pi D/(4\sqrt{AK}) = 0.8$ (A.16). The calculated profiles $\theta(r,\ a)$ and the corresponding curves $\theta_r(\theta)$ in the interval $[0.4 < a < 4.0]$ are plotted in figures 3(c), (d). Most of curves $\theta(r,\ a)$ oscillate near lines $\theta_{1,2} = \pm\pi/2$, the maximum values of $w_a = K\sin^2\theta$, and the corresponding profiles $\theta_r(\theta)$ spiral around the *attractors*, points $(\pm\pi/2,\ 0)$. Among these curves there is a singular line (with $a = 1.62471$) which ends in the *saddle* point $(0,\ 0)$ and, thus, represents a solution of the boundary value problem for isolated skyrmions.

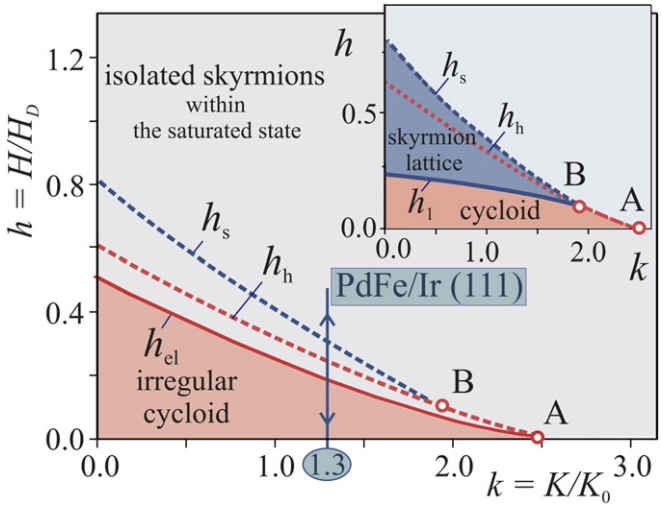

Figure 4. In the phase diagram in variables k and h the existence area of metastable isolated skyrmions is restricted by the strip-out critical line $h_{el}(k)$. The inset shows the regions of global stability of the modulated (helicoidal and skyrmion lattice) and the spatially homogeneous saturated phases (for details see [17]).

The visual representation of the solutions for the auxiliary Cauchy problem (13), (19) as parametrized profiles $\theta(r,\ a)$ (figure 3(c)) and $\theta_r(\theta)$ curves in $(\theta,\ \theta_r)$ phase plane (figure 3(d)) reveal mathematical regularities in the formation of the localized states.

To demonstrate a crucial role of the DM interactions in the stabilization of chiral skyrmions, in the following we compare the phase portrait in figure 3(d) with special cases of model (12) with $D = 0$.

Isotropic ferromagnets ($D = K = H = 0$). The Euler equations for energy functional of an isotropic ferromagnet $w = A\,(\mathbf{grad\ m})^2$ yield rigorous analytical solutions for axisymmetric skyrmions $\theta(r)$, $\psi(\varphi)$ derived by Belavin and Polyakov [52]

$$\psi = N\varphi + \alpha, \quad \tan(\theta/2) = (\delta/r)^N, \tag{20}$$

where α and $\delta > 0$ are arbitrary values and N are positive integers. The energy (11) for solutions (20) $\mathcal{F}_0 = 8\pi AN$, does not depend on values δ and α [52]. For $N = 1$ a set of magnetization profiles $\theta(r/\delta)$ (20) and phase portrait trajectories $\theta_r(\theta)$

$$\theta = 2\arctan(\delta/r), \quad \delta\theta_r = -2\sin^2(\theta/2), \tag{21}$$

are plotted in figure 5. For $\delta > 0$, the curves $\theta_r(\theta)$ start in points $(\pi,\ -2/\delta)$ and end in the saddle point $(0,\ 0)$. However, any anisotropy or magnetic field will destabilize this solution.

Uniaxial centrosymmetric ferromagnets ($D = 0$). In this case equation (13) has no stable solutions for isolated skyrmions. For $H > 0$ all phase trajectories $\theta_r(\theta)$ spiral around attractor $(-\pi/2,\ 0)$. For $H < 0$ equation (13) has radially unstable solutions for isolated skyrmions as proved by Derrick-Hobart theorem (For details see [3, 10]).

2.2.2. Derrick scaling identities and a virial theorem for chiral skyrmions

Analysis of skyrmion energy $\mathcal{F}$ (11) under scaling transformations offers further important insight into the physics of chiral skyrmions. We consider a family of functions $\vartheta(r) = \vartheta(r/\eta)$ obeying the boundary conditions (14). Here $\eta > 0$ is an arbitrary constant describing uniform compressions $(0 < \eta < 1)$ or expansions $(\eta > 1)$ of profile $\vartheta(r)$. For rescaled functions $\vartheta(r) = \vartheta(r/\eta)$, the skyrmion energy $\widetilde{\mathcal{F}}$ (11) can be expressed as a function of η:

$$\widetilde{\mathcal{F}}(\eta) = \mathcal{E}_e - \mathcal{E}_D\eta + \mathcal{E}_0\eta^2. \tag{22}$$

The values of the exchange ($\mathcal{E}_e$), Dzyaloshinskii-Moriya ($\mathcal{E}_D$), and potential ($\mathcal{E}_0$) energy contributions for profile $\vartheta(r)$ (11) are given as follows:

$$\mathcal{E}_e = 2\pi A\int_0^\infty\left(\vartheta_\xi^2 + \frac{1}{\xi^2}\sin^2\vartheta\right)\xi\mathrm{d}\xi \equiv A\alpha_1,$$

$$\mathcal{E}_D = 2\pi|D|\int_0^\infty\left(\vartheta_\xi + \frac{1}{\xi}\sin\vartheta\cos\vartheta\right)\xi\mathrm{d}\xi \equiv |D|\alpha_2,$$

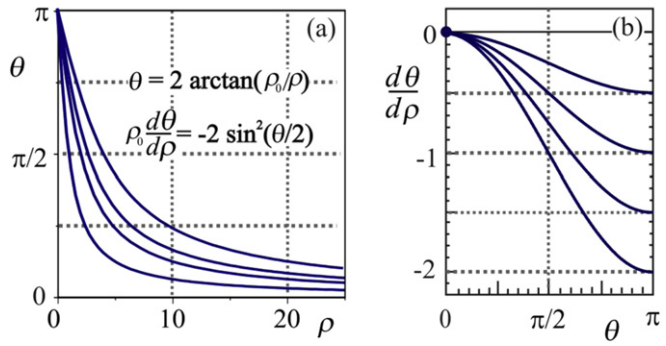

Figure 5. Magnetization profiles for Belavin-Polyakov instantons (a) and the corresponding phase portraits of the solutions (b).

$$\mathcal{E}_0 = 2\pi \int_0^\infty [K \sin^2 \vartheta + \mu_0 MH (1 - \cos \vartheta)] \xi d\xi \tag{23}$$

or $\mathcal{E}_0 = K\alpha_3 + \mu_0 MH\alpha_4$, where α_i are the numerical coefficients given by the values of the integrals in equation (23).

Equation (22) shows that the DM energy plays a crucial role in stabilizing skyrmions [2, 13]. In centrosymmetric ferromagnets ($\mathcal{E}_D = 0$) isolated skyrmions are unstable with respect to compression and collapse into a singular line ($\eta \to 0$) (*Derrick-Hobard* theorem [10]). Skyrmion solutions that minimize the free energy (22) only occur for nonzero Dzyaloshinskii-Moriya energy contributions.

Ansatz solutions. Potential $\widetilde{\mathcal{F}}(\eta)$ (22) has a convenient form for analysis of skyrmion solutions with trial functions of type $\vartheta = \vartheta(\rho/\eta)$ that obey the boundary conditions (14). Particularly, a linear ansatz

$$\vartheta = \pi [1 - (r/\eta)] \quad (r < \eta), \qquad \vartheta = 0 \quad (r > \eta), \tag{24}$$

has been used in [2] to introduce the phenomenon of chiral skyrmions. The ansatz,

$$\vartheta(r/\eta) = 4 \arctan [\exp(-r/\eta)], \tag{25}$$

based on solutions for isolated 360° Bloch walls [38] provides a good fit to the solutions of equation (13). In [32], magnetization profiles for isolated skyrmions have been fitted by a combination of functions of type (25). For the trial function $\vartheta(r/\eta)$ in equation (25), the total energy (22) can be written as

$\mathcal{F}(\eta)/(2\pi) = 4.31A + (1.59K + 1.39\mu_0 MH)\eta^2 - 3.02D\eta$. For zero anisotropy ($k = 0$) this ansatz yields the transition field into the skyrmion lattice $h_s = H_s/H_D = 0.760$ (cf. with the rigorous value $h_s = 0.801$ and $h_s = 0.675$ for the linear ansatz (24) [2]).

For $\widetilde{\mathcal{F}}(\eta)$ (22) the equilibrium skyrmion size is

$$\eta_0 = \frac{L_D}{2\pi} \frac{\alpha_2}{\alpha_3 k + 2\alpha_4 h}, \tag{26}$$

expressed as a ratio of the Dzyaloshinskii-Moriya to the potential energy contributions for the trial function.

The *virial* theorem for isolated axisymmetric skyrmions is derived by integration of the Euler equation (13). Partial integration leads to the following *virial* relation between the equilibrium values of the potential and DM energies [33] $\bar{\mathcal{E}}_0 = 2\bar{\mathcal{E}}_D$ where $\bar{\mathcal{E}}_0$, $\bar{\mathcal{E}}_D$ are the integrals (23) calculated for the solutions of equation (13), $\vartheta = \theta(\rho)$.

2.2.3. Radial stability and collapse at high field (discrete model)

The stability of the solutions $\theta(\rho)$ of the boundary value problem (13), (14) under small radial distortions $\zeta(\rho)$ ($\zeta(0) = \zeta(\infty) = 0$) has been investigated in [14]. This problem is reduced to the spectral problem for the perturbation energy functional [14]. By numerically solving the eigenvalue problem for this functional, the radial stability of isolated skyrmions has been established in a broad range of the control parameters (k, h) [3]. Contrary to magnetic bubbles, which collapse with finite radii at certain critical fields [38], the solutions of the boundary value problem (13) and (14) (figure 3) exist at arbitrary high fields. In increasing fields their sizes gradually decrease and asymptotically approach zero.

The continuum model (2), however, becomes invalid for localized solutions with sizes of few lattice constants. In this region we investigate solutions for chiral skyrmions within the discrete models. We consider classical spins, $\mathbf{S}_i$, of unit length on a two-dimensional square lattice with the following energy functional [47] $E = E_0 + E_D$ where

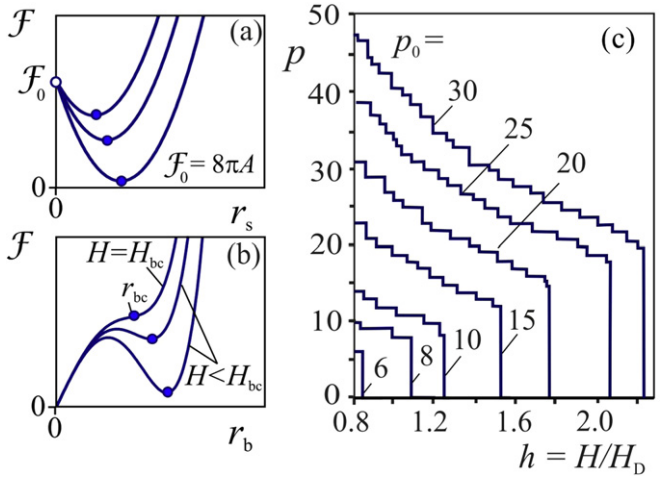

Figure 6. Micromagnetic energies of an isolated skyrmion (a) and a bubble-domain (b) as function of their sizes for selected values of the applied magnetic fields [14, 38]. Isolated bubbles collapse at critical field H_{bc} with finite radius r_{bc}. Isolated chiral skyrmions exist at very high fields without collapse. The equilibrium skyrmion sizes p as functions of the applied field calculated for different values of p_0 (30) indicate the collapse of chiral skyrmions (c) (p is defined here as a diameter of a circle encompassing a skyrmion core area with $m_z \leqslant 0.995$).

$$E_0 = -J \sum_{\langle i,j \rangle} (\mathbf{S}_i \cdot \mathbf{S}_j) - \sum_i [\mathbf{H} \cdot \mathbf{S}_i + K (\mathbf{S}_i \cdot \mathbf{n})^2], \tag{27}$$

and the Dzyaloshinskii-Moriya energy equals

$$E_D = -D \sum_i (\mathbf{S}_i \times \mathbf{S}_{i+\hat{x}} \cdot \hat{x} + \mathbf{S}_i \times \mathbf{S}_{i+\hat{y}} \cdot \hat{y}) \tag{28}$$

for Bloch-type modulations, and

$$E_D = -D \sum_i (\mathbf{S}_i \times \mathbf{S}_{i+\hat{x}} \cdot \hat{y} - \mathbf{S}_i \times \mathbf{S}_{i+\hat{y}} \cdot \hat{x}) \tag{29}$$

for Néel-type modulations ($\langle i, j \rangle$ denotes pairs of nearest-neighbor spins).

For a helix $\mathbf{S}_i = (\cos\theta_i, \sin\theta_i, 0)$ propagating along the x-axis at field and anisotropy ($\mathbf{H} = K = 0$), model (27) is reduced to

$$E = \sum_i [-J \cos(\theta_i - \theta_{i+\hat{x}}) - D \sin(\theta_i - \theta_{i+\hat{x}})], \tag{30}$$

and yields the equilibrium period $p_0 = 2\pi/\arctan(D/J)$ (p_0 is the number of magnetic ions corresponding to $\Delta\theta = 2\pi$).

The equilibrium solutions for isolated skyrmions are derived by numerically solving the equations minimizing the energy functional E (27). Typical solutions for the equilibrium skyrmion size p as a function of the applied field are plotted in figure 6(c). The solutions with finite sizes exist only below a certain critical (*collapse*) field $h_c(p_0)$ (figure 6(a)). The critical field $h_c(p_0)$ increases without limit with increasing p_0 (figure 6(b)) and, thus, signifies a transition from the discrete model to the continuous model.

2.2.4. Elliptic instability (strip-out) at low fields

Isolated skyrmions exist as metastable states above the critical field $h_s(k)$ (figures 4(a), (b)). Below this line the energy $\mathcal{F}$ (11) becomes negative and skyrmions tend to condense into a hexagonal lattice [3]. However, if the formation of skyrmion lattices is suppressed (as in PdFe/Ir (111) films [32]) isolated skyrmions continue to exist below the critical line $h_s(k)$ (with the skyrmion core energy density lower than that of the surrounding saturated state). At the same time isolated skyrmions have a tendency to elongate and expand into a band with helicoidal or cycloidal modulations and eventually to fill the whole space, since the spiral state represents the minimum with lower energy as compared to the local minima with the metastable isolated skyrmions. These (*elliptic*) instabilities are similar to 'strip-out' instabilities of isolated magnetic bubbles at a certain critical field [53] observed in common 'bubble-domain' films [38] and in magnetic nanolayers with perpendicular anisotropy [54]. A theory of elliptic instabilities for chiral skyrmions have been developed in [33] where a strip-out field has been derived from the stability analysis of the skyrmion energy (11) with respect to (elliptic) perturbations of type

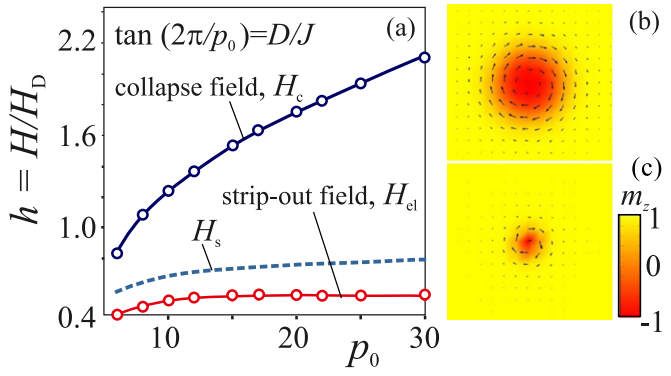

Figure 7. Collapse (H_c) and strip-out or elliptic instability (H_{el}) critical fields calculated within the discrete model (27) for $k = 0$ and different values of p_0 (30). At the dashed line $H_s(p_0)$ the isolated skyrmion energy $\mathcal{F}$ equals zero, and below this line skyrmions can condense into the hexagonal lattice (a). Calculated distributions of the magnetization of the skyrmion core for $k = 1.315$, $p_0 = 24$ and for $h = 0.42$ (b) and $h = 1.27$ (c).

$$\tilde{\rho} = \rho + \varepsilon\eta(\rho)\cos 2\varphi, \quad \tilde{\psi} = \psi + \zeta(\rho, \varphi), \tag{31}$$

where ($\varepsilon \ll 1$)[33] . In [33], the strip-out field H_{el} has been calculated for stray-field free elliptic distortions of Bloch-type isolated skyrmions. There, a set of parametrized ansatz functions of type $\eta(\rho) = \sin\theta/(1 + a\sin\theta)$ with optimized values of a were used [33]. In this paper the critical line $h_{el}(k)$ ($0 < k < k_a$) for a Bloch-type-skyrmion (figure 4) has been calculated by direct minimization of the perturbation energy.

Within the discrete model (27) the critical field h_{el} has been calculated for zero anisotropy ($k = 0$) and for $6 < p_0 < 30$. Figure 7 (a) shows that the strip-out field h_{el} essentially decreases with the decreased size of skyrmions what can be beneficial for possible application of such skyrmions. However, the existence region of these isolated skyrmions is restricted by the lower field of collapse h_c.

2.2.5. The k — h phase diagrams

In this section we consider the existence area for isolated skyrmions in the magnetic phase diagram (figure 4). The energy functional for uniaxial chiral ferromagnets (2) depends on the two independent control parameters, the reduced values of the applied field, h and uniaxial anisotropy, k (15). The magnetic phase diagram in variables k and h collects *all* possible solutions for model (2). The calculated phase diagram in the inset of figure 4 shows the existence areas of the cycloids and skyrmion lattices and the transition lines between these modulated phases and the saturated state. The phase diagram indicates the critical fields at zero anisotropy, the bicritical point B (1.90, 0.10), and the critical point A (2.67, 0) [3] (for a detailed description of this phase diagram see [17]). Figure 4 shows critical lines for isolated skyrmions (results of the continuum model (2)). Isolated skyrmions condense into a skyrmion lattice when the applied magnetic field decreases to the critical value $h_s(k)$. However, isolated skyrmions can exist as localized objects below the critical line $h_s(k)$ and strip-out into helicoids at the critical line h_{el}.

3. Experiment: isolated skyrmions in PdFe/Ir(111) bilayers

Sample preparation and spin-polarized (SP)- STM experiments were performed in a multi-chamber UHV system at a base pressure of $5 \cdot 10^{-11}$ mbar. Details of the sample preparation can be found in [31]. We use antiferromagnetic bulk Cr tips to minimize magnetostatic interactions between tip and sample. The SP-STM measurements were performed at $T = 4.2$ K in perpendicular magnetic fields of -3 to $+3$ Tesla. We repeatedly scanned the same sample area while continuously sweeping the magnetic field at a speed of 12.8 mT/min, resulting in a series of images with a field difference of $\Delta B = 87$ mT. Constant current images and maps of differential conductance (dI/dU) were measured simultaneously by lock-in technique. All SP-STM images displayed in this work are dI/dU maps. We used small bias voltages ($U = 20$mV) and moderate currents ($I = 3$ nA) to minimize the influence of the tunnel process on the field-dependent magnetic evolution within the PdFe bilayer [31].

PdFe/Ir(111) bilayers have a uniaxial anisotropy of 'easy-axis' type and exhibit chiral modulations of Néel-type [31, 32]. It was also established by SP-STM observations that a cycloid (figure 2(b)) is the ground state of PdFe/Ir(111) films [31]. The material parameters of model (2) for PdFe/Ir(111) at $T = 4.2$ K determined in [32, 55] yield the following values for the characteristic parameters (16): $L_D = 6.44\,\text{nm} = 23.85a_0$ i.e. $p_0 = 24$ ($a_0 = 0.27$ nm is the lattice constant), $\mu_0 H_D = 3.46$ T, $K_0 = 1.9 \times 10^6$ J/m^3, $K_d = \mu_0 M^2/2 = 0.76 \times 10^6$ J/

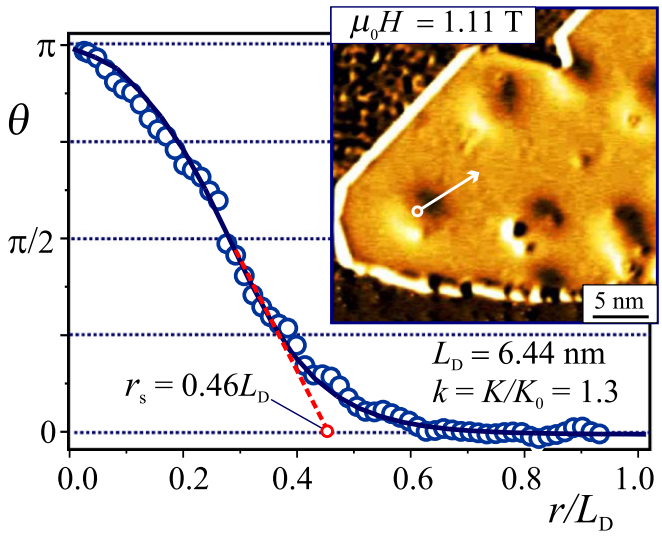

Figure 8. Magnetization profile $\theta(r)$ for an isolated skyrmion (circles) derived from SP-STM data (inset) for the applied field $\mu_0 H = 1.11$ T. Data has been taken along the arrow in the inset. The profile $\theta(r)$ can be directly calculated after determining the tip magnetization direction by fitting a trial function to the skyrmion profile[32]. The solid line is the solution of equation (17) for $k = 1.315$ and $h = 0.321$, r_s is the skyrmion core radius defined by equation (18).

m^3 ('shape anisotropy'). The sufficiently strong values of 'easy-axis' anisotropy ($k = K/K_0 = 1.315$) ensures the stability of chiral modulations in PdFe/Ir(111) films with respect to stray-field effects [34, 38] and make them convenient objects for investigations of chiral skyrmions [31, 32].

The calculated magnetic phase diagram of easy-axis chiral ferromagnets includes the existence areas of one-dimensional modulations and skyrmion lattices (figure 4, Inset) [3, 17]. These chiral modulations and transitions between them have been directly observed by Lorentz transmission electron microscopy (LTEM) in free standing nanolayers of cubic helimagnets [23, 24, 29, 30] and in PdFe/Ir(111) bilayer films by SP-STM [31, 32].

Isolated skyrmions and their internal structure have been investigated by SP-STM in PdFe bilayers [31, 32]. Following [32] we reconstruct the magnetization profile $\theta(r)$ for one of the isolated skyrmions in the film at the applied field $\mu_0 H = 1.11$ T (figure 8). These experimental results are in close agreement with the solution of equation (17) for $k = 1.315$ and $h = 0.321$ (or $\mu_0 H = 1.11$ T). In free standing films of magnetically soft cubic helimagnets, chiral skyrmions readily condense into hexagonal lattices below $h_s(k)$ (figure 4, inset) [23, 24, 30, 31]. At low temperatures, however, an enhanced coercitivity of PdFe/Ir (111) bilayers prevents the formation of skyrmion lattices below $h_s(k)$ (see the results of [32] for $T = 4.2$ K). This offers a unique opportunity to investigate isolated skyrmions in a broad range of applied fields.

Figure 9 shows selected frames from the whole SP-STM data set where the evolution from isolated skyrmions at high fields to spin spirals at zero field can be observed. The two-lobe appearance of skyrmions is due to a predominantly in-plane magnetization of the Cr tip [31, 32]. The strip-out of skyrmions starts in figure 9(c) where a skyrmion, labeled (1), has jumped to a different position and a skyrmion (2) has developed an elongated shape. In figure 9(f) more skyrmions have adopted elongated shapes, a process that seems to be influenced and assisted by defects, see skyrmion (3), and the repulsive interactions with other skyrmions and chiral modulations along the sample edges (so called *surface twists*) [35, 56]. The strip-out process can be quantified more accurately in an area with only one strongly pinning defect, see detailed view in figure 10. In figure 10(c) the skyrmion shape starts to deviate from rotational symmetry at $\mu_0 H \approx 1.1$ T and becomes more and more elongated through figures 9(d) and (e). Other skyrmions retain axial symmetry even at much lower fields. The calculated value of the strip-out field for $k = 1.315$ equals $\mu_0 H_{el} = 0.65$ T. The images in figure 9 (see also video materials in [32]) show that the elliptical instability field has different values for different skyrmions and strongly depends on skyrmion-skyrmion interactions, interactions with sample edges and defects. Similar effects are characteristic for strip-out instabilities of isolated bubble domains (see e.g. [54]).

To determine the skyrmion collapse field with reasonable statistical accuracy, we have monitored the repeated creation and annihilation of a skyrmion at higher tunnel bias and current as a function of applied field. With the tip positioned above the pinning defect, we monitored the telegraph noise in the spin-resolved dI/dU signal and extracted the average lifetime of the skyrmion as a function of applied field (see insets in figure 11). The skyrmion lifetime decreases roughly exponentially [57] down to a value of 5 ms at 4.5 T reaching the time

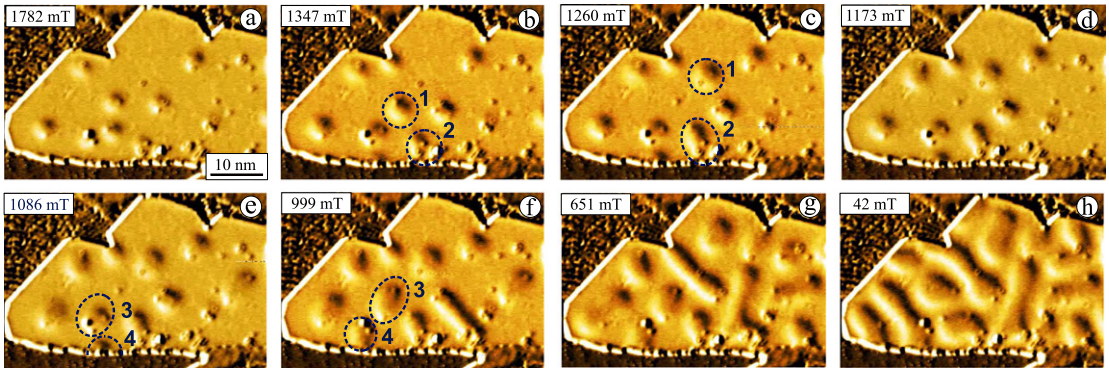

Figure 9. Field-dependent dI/dU maps of PdFe/Ir(111) taken at $T = 4.2$ K, $U = 20$ mV and $I = 3$ nA. The extension of elliptic deformations in isolated skyrmions in decreasing applied magnetic fields (a-f) is terminated by the formation of cycloid patterns (g, h).

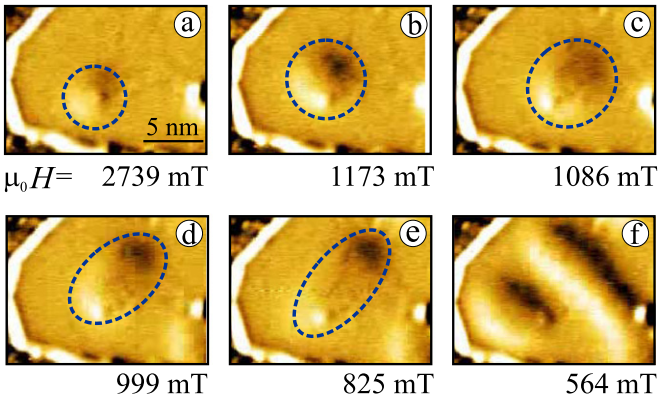

Figure 10. Detailed view of an isolated skyrmion. With decreasing external magnetic field the skyrmion gradually develops an elliptical shape and finally stretches into a spiral domain.

resolution limit of our setup. At this field value the skyrmion state is still metastable and the collapse field must therefore be higher than 4.5 T.

Minimization of functional (27) with $p_0 = 24$ and $k = 1.315$ yields the collapse field 4.4 T, in reasonable agreement with the experimental data.

4. Conclusions

Detailed SP-STM investigations of magnetic states in PdFe/Ir (111) thin films and a comprehensive theoretical analysis within the standard model (2) enable to describe the basic magnetic properties of isolated chiral skyrmions and describe their evolution in a broad range of applied magnetic fields.

The equilibrium states of isolated axisymmetric skyrmions are described by differential equation (17) *common* for different groups of chiral magnets [2, 3]. Moreover, similar equations describe axisymmetric solitonic states in other condensed matter systems with broken inversion symmetry [15] including noncentrosymmetric antiferromagnets [68, 69] and chiral liquid crystals [58–60].

This implies a universal character of chiral skyrmion properties and allows to consider the investigations in PdFe/Ir films as representative of the entire phenomenon. These investigations include general features of the chiral skyrmion evolution in applied magnetic fields terminated at lower fields by the formation of skyrmion condensates or by elliptic instabilities of individual skyrmions and the collapse of the skyrmion core at high fields.

In this paper we have investigated magnetic properties of solitary skyrmions only and neglected their interactions with other skyrmions, with chiral modulations arising at the sample edges[56], and different types of defects. We also have considered skyrmions magnetically homogeneous along their axis. This assumption is justified by the structure of PdFe/Ir (111) bilayers that exclude magnetic modulations along the film thickness

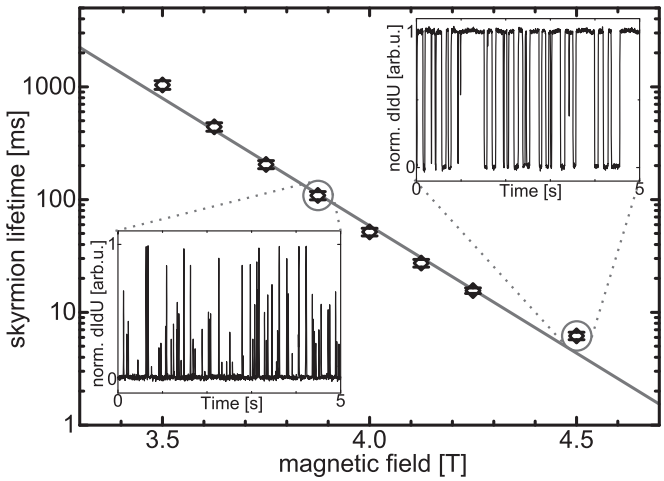

Figure 11. Skyrmion lifetime as a function of external magnetic field at $T = 4.2$ K. Data points are derived from telegraph noise (see insets) measured with the SP-STM tip held stationary above the pinning defect at $U = +600$ mV, $I = 100$ nA. The lifetime is still finite at $\mu_0 H = 4.5$ T, which means that the collapse field is above this value.

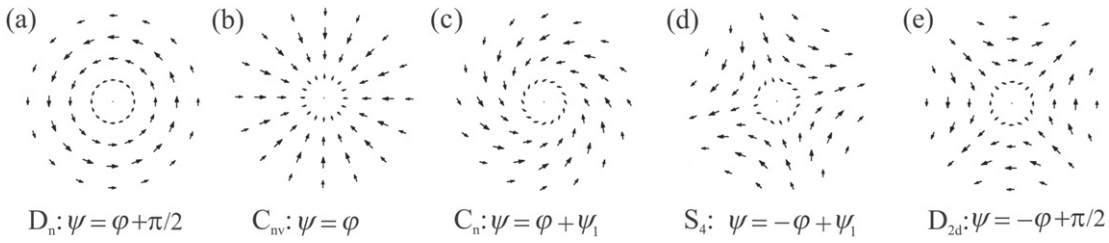

Figure 12. Projections of **m** onto the basal plane in the core of chiral skyrmions for noncentrosymmetric uniaxial ferromagnets [2].

[2]. In thicker cubic helimagnets and uniaxial ferromagnets with D_n and C_n symmetry, however, such modulations are physically admissible and influence magnetic properties of these systems [35, 56].

Recently chiral skyrmions and bubble domains have been investigated in magnetic multilayers with a strong easy-axis magnetic anisotropy [54, 65–67]. In such systems, the interlayer exchange and dipole couplings play an important role in the formation of the equilibrium magnetic states. Stray fields for bubble domains in magnetic multilayers have been calculated and investigated in [54]. In a similar way, the equilibrium magnetic configurations and stray-field energy can be derived for chiral skyrmions by applying methods and results of [34, 39, 40, 54].

Acknowledgments

AOL acknowledges financial support by the FOM grant 11PR2928. NR, AK, and RW acknowledge support by the Deutsche Forschungsgemeinschaft via SFB668-A8, and ANB via Grant No. BO 4160/1-1.

Appendix

A.1. Skyrmion structure in different classes of uniaxial helimagnets

Functional forms of w_D energy contributions are determined by crystallographic symmetry of a noncentrosymmetric magnetic crystal [1, 2, 61].

$$w_1^{(\pm)} = \mathcal{L}_{zx}^{(x)} \pm \mathcal{L}_{zy}^{(y)}, \quad w_2^{(\pm)} = \mathcal{L}_{zx}^{(y)} \pm \mathcal{L}_{zy}^{(x)}, \tag{A.1}$$

$$C_{nv} : [w_1^{(+)}], \quad D_{2d} : [w_1^{(-)}], \quad D_n : [w_2^{(-)}, \mathcal{L}_{xy}^{(z)}],$$
$$S_4 : [w_1^{(-)}, w_2^{(-)}], \quad C_n : [w_1^{(+)}, w_2^{(+)}, \mathcal{L}_{xy}^{(z)}]. \tag{A.2}$$

For $\theta(\rho,\,\varphi)$, $\psi(\rho,\,\varphi)$

$$w_1^{(+)} = \cos(\psi-\varphi)\theta_\rho - \sin\theta\cos\theta\sin(\psi-\varphi)\psi_\rho - \frac{1}{\rho}\sin(\psi-\varphi)\theta_\varphi + \frac{1}{\rho}\sin\theta\cos\theta\cos(\psi-\varphi)\psi_\varphi \quad (A.3)$$

$$w_1^{(-)} = \cos(\psi+\varphi)\theta_\rho - \sin\theta\cos\theta\sin(\psi+\varphi)\psi_\rho - \frac{1}{\rho}\sin(\psi+\varphi)\theta_\varphi - \frac{1}{\rho}\sin\theta\cos\theta\cos(\psi+\varphi)\psi_\varphi \quad (A.4)$$

$$w_2^{(+)} = \sin(\psi-\varphi)\theta_\rho - \sin\theta\cos\theta\cos(\psi-\varphi)\psi_\rho + \frac{1}{\rho}\cos(\psi-\varphi)\theta_\varphi - \frac{1}{\rho}\sin\theta\cos\theta\sin(\psi-\varphi)\psi_\varphi \quad (A.5)$$

$$w_2^{(-)} = \sin(\psi+\varphi)\theta_\rho - \sin\theta\cos\theta\cos(\psi+\varphi)\psi_\rho + \frac{1}{\rho}\cos(\psi+\varphi)\theta_\varphi - \frac{1}{\rho}\sin\theta\cos\theta\cos(\psi+\varphi)\psi_\varphi \quad (A.6)$$

The solutions $\psi(\phi)$ are determined by crystal classes of the system [2].

$$C_{nv}:\psi=\varphi,\quad D_{2d}:\psi=-\varphi+\pi/2,\quad D_n:\psi=\varphi+\pi/2,$$
$$S_4:\psi=-\varphi+\psi_1,\quad C_n:\psi=\varphi+\psi_1. \quad (A.7)$$

For ferromagnets belonging to S_4 and C_n classes energy functionals w_D include two terms: $w_D = D_1 w_1^{(-)} + D_2 w_2^{(-)}$ for S_4 and $w_D = D_1 w_1^{(+)} + D_2 w_2^{(+)}$ for C_n. Angles $\psi_1 = \arctan(D_2/D_1)$ and the effective values of the DM constant are $D = \sqrt{D_1^2 + D_2^2}$.

For noncentrosymmetric cubic ferromagnets belonging to T and O crystallographic classes the energy functional w_D has the following form [61]

$$w_D = \mathcal{L}_{yx}^{(z)} + \mathcal{L}_{xz}^{(y)} + \mathcal{L}_{zy}^{(x)} = \mathbf{m}\cdot\mathrm{rot}\mathbf{m}, \quad (A.8)$$

and stabilizes solutions with $\psi = \pi/2 + \varphi$.

The skyrmion energy densities for all these structures can be reduced to a common functional form [3].

A.2. Solutions for one-dimensional modulations

For one-dimensional modulations propagating along the $\xi-$ axis the energy functional (2) can be written as

$$w = A(\theta_\xi^2 + \sin^2\theta\psi_\xi^2) + w_D - K\cos^2\theta - \mu_0 MH\cos\theta. \quad (A.9)$$

In the DM energy contribution w_D (A.9) Lifshitz invariants of type $\mathcal{L}_{ij}^{(x)}$, $\mathcal{L}_{ij}^{(y)}$ induce modulations propagating in the *xy* plane (e.g. *helicoids* and *cycloids* in figures 2(a), (b)), and invariants $\mathcal{L}_{xy}^{(z)}$ favour modulations along the *z*-axis (*cones*).

Helicoids and cycloids. To be specific, we consider in-plane modulations propagating along the $x-$ axis. Depending on the magnetic crystal symmetry, different types of modulations are stabilized by the w_D energy functional [2]. Particularly, in cubic helimagnets and uniaxial ferromagnets of D_n crystallographic classes, **M** rotates as a Bloch-type domain wall (*helicoids*), and in uniaxial ferromagnets with C_{nv} symmetry the magnetization rotates along the propagation direction like a Néel-type domain wall (*cycloids*) (figures 2(a), (b)):

$$\mathbf{m} = \vec{e}_y\sin\theta\,(x) + \vec{e}_z\cos\theta\,(x) \quad \text{(helicoids)},$$
$$\mathbf{m} = \vec{e}_y\sin\theta\,(x) + \vec{e}_z\cos\theta\,(x) \quad \text{(cycloids)}. \quad (A.10)$$

The Euler equation for the functional

$$w_\mathrm{h}(\theta) = A\theta_x^2 - D\theta_x - \mu_0 MH\cos\theta - K\cos^2\theta \quad (A.11)$$

yields magnetization profiles $\theta(x)$ for helicoids and cycloids [1]. Analytical solutions for $\theta(x)$ describe helical modulations distorted by the applied field and uniaxial anisotropy [1]. These helicoids (cycloids) gradually unwind into a set of isolated domain walls at critical line $H_\mathrm{h}(K)$ [1, 3, 17].

Cones. In cubic helimagnets and uniaxial ferromagnets with C_n and D_n symmetries, the DM energy functional w_D includes Lifshitz invariants $\mathcal{L}_{xy}^{(z)}$ (A.2), (A.8) favouring chiral modulations (*cone* phases) along the $z-$ axis. Minimization of the energy functional

$$w_\mathrm{h}(\theta) = A\theta_z^2 - D\theta_z - \mu_0 MH\cos\theta - K\cos^2\theta \quad (A.12)$$

yields the solutions for single-harmonic modulations describing the cone phase [42, 61]:

$$\cos\theta = \frac{H}{H_D}\left(1 - \frac{K}{K_0}\right)^{-1}, \quad \psi = z/L_D. \tag{A.13}$$

These equations include the characteristic parameters of a uniaxial chiral ferromagnet (16).

A.3. Characteristic lengths and critical parameters

In uniaxial noncentrosymmetric ferromagnets, chiral modulations arise as a result of a competition between the DM interactions favouring a rotation of the magnetization, the exchange coupling and the 'potential' energy $f(\theta) = -\mu_0 MH\cos\theta - K\cos^2\theta$ tending to suppress such modulations. The balance between the chiral energy $w_D(\theta, \theta_\rho)$ and the potential energy contributions $f(\theta)$ determine the equilibrium spin configurations in chiral magnets. At zero field and for zero anisotropy single-harmonic modulations $\theta = q_0 x$ ($q_0 = D/(2A)$) minimize the functional (A.9). In the opposite limit of strong anisotropy ($K > \pi^2 D^2/(16A)$) these modulations transform into a set of isolated 180° domain walls separating the homogeneous states with $\theta_1 = 0$, $\theta_2 = \pi$.

The width of an isolated Bloch domain wall L_B, its energy, γ_B, and anisotropy field H_a are as follows:

$$L_B = \pi\sqrt{\frac{A}{K}}, \quad \gamma_B = 4\sqrt{AK}. \quad H_a = \frac{K}{\mu_0 M_0} \tag{A.14}$$

These are the fundamental parameters describing magnetic states in a common (centrosymmetric) uniaxial ferromagnet [38]. To demonstrate a competing character of the magnetic interactions in chiral uniaxial ferromagnets, we consider an isolated domain wall at zero field that separates the homogeneous states with $\theta_1 = 0$ and $\theta_2 = \pi$. The equilibrium states of this domain wall are derived by minimization of functional (A.9) for $H = 0$ [38]. The standard calculation of the wall energy [38] $\gamma_w = \int_0^\infty [w_h(\theta) - w_h(0)]\,dx$ yields the following result [3, 62]

$$\gamma_w = 4\sqrt{AK} - \pi|D| = 4\pi A\left(\frac{1}{L_B} - \frac{\pi}{L_D}\right). \tag{A.15}$$

The first (positive) term in (A.15) is the wall energy of a uniaxial ferromagnet [38] arising as a common effect of the uniaxial anisotropy pinning the magnetization vector along the easy-axis and the exchange stiffness suppressing deviations of **M** from these directions. The negative energy contribution in γ_w (A.15) is due to the DM interactions favouring modulations of the magnetization with a specific rotation sense. The strength of this 'winding force' is characterized by $1/L_D$: the larger the DM coupling, the smaller the period of the modulations. For $L_D < \pi L_B$ the wall energy becomes negative manifesting the instability of the homogeneous states with respect to chiral modulations.

The dimensionless parameter $\varkappa$ introduced as [3, 62]

$$\gamma_w = 4\sqrt{AK}(1 - \varkappa), \quad \varkappa = \frac{\pi}{4}\frac{|D|}{\sqrt{AK}} = \frac{\pi L_B}{L_D}, \tag{A.16}$$

provides the criterion for the existence of chiral modulated states. For $\varkappa > 1$, the DM interactions overcome a pinning of the magnetization along easy-axis direction and stabilize modulated states. For $0 < \varkappa < 1$ chiral modulated phases are totally suppressed, and chiral patterns exist as metastable localized states in a form of isolated skyrmions and domain walls (kinks).

Parameter $\varkappa$ (A.16) is similar to the *Ginzburg-Landau parameter* $\varkappa_{GL} = \lambda/\xi$ in the theory of Abrikosov vortices (the mixed state) in superconductors [63]. The parameter $\varkappa_{GL}$ is a ratio of two characteristic lengths, the *coherence length* ξ and the *penetration depth* λ. Abrikosov vortices exist in superconductors with $\varkappa_{GL} > 1/\sqrt{2}$ (*type-II superconductors*) [63, 64]. Physical analogies between superconductor's mixed states and chiral magnetic modulations are discussed in [3, 62]. The characteristic lengths L_D and L_B provide different ways to introduce reduced variables into model (12).

The reduced energy functional based on the characteristic length L_B with control parameters $\tilde{h} = H/H_a$ and $\varkappa$ (A.16) and the reduced magnetic field (where H_a define in equation (A.14) is convenient for investigations of isolated skyrmions in helimagnets with a strong uniaxial anisotropy ($0 < \varkappa < 1$) [33, 34].

References

[1] Dzyaloshinskii I E 1964 *Sov. Phys. JETP* **19** 960
Dzyaloshinskii I E 1964 *Sov. Phys. JETP* **20** 665
[2] Bogdanov A N and Yablonskii D A 1989 *Zh. Eksp. Teor. Fiz.* **95** 178
Bogdanov A N and Yablonskii D A 1989 *Sov. Phys. JETP* **68** 101 (http:/etp.ac.ru/cgi-bin/e/index/r/95/1/p178?a = list)
Bogdanov A N, Kudinov A V and Yablonskii D A 1989 *Sov. Phys. Solid State* **31** 1707
[3] Bogdanov A and Hubert A 1994 *J. Magn. Magn. Mater.* **138** 255

[4] Rößler U K, Leonov A A and Bogdanov A N 2011 *J. Phys.: Conf. Ser.* **303** 012105
[5] Rajaraman R 1987 *Solitons and Instantons* (Amsterdam: North Holland)
[6] Manton N and Sutcliffe P 2004 *Topological Solitons* (Cambridge: Cambridge University Press)
[7] Brown G E and Rho M (ed) 2010 *The Multifaceted Skyrmion* (Singapore: World Scientific)
[8] Melcher C 2014 *Proc. R. Soc.* A **470** 20140394
[9] Cross M C and Hohenberg P C 1993 *Rev. Mod. Phys.* **65** 851
[10] Derrick G H 1964 *J. Math. Phys.* **5** 1252
[11] Skyrme T H 1961 *Proc. R. Soc.* A **260** 127
[12] Leonov A O and Mostovoy M 2015 *Nat. Commun.* **6** 8275
[13] Bogdanov A 1995 *JETP Lett.* **62** 247
[14] Bogdanov A and Hubert A 1999 *J. Magn. Magn. Mater.* **195** 182
[15] Rößler U K, Bogdanov A N and Pfleiderer C 2006 *Nature* **442** 797
[16] Wilhelm H, Baenitz M, Schmidt M, Roessler U K, Leonov A A and Bogdanov A N 2011 *Phys. Rev. Lett.* **107** 127203
[17] Wilson M N, Butenko A B, Bogdanov A N and Monchesky T L 2014 *Phys. Rev.* B **89** 094411
[18] Wilhelm H, Baenitz M, Schmidt M, Naylor C, Lortz R, Roessler U K, Leonov A A and Bogdanov A N 2012 *J. Phys.: Condens. Matt.* **24** 294204
[19] Keesman R, Leonov A O, Buhrandt S, Barkema G T, Fritz L and Duine R A 2015 *Phys. Rev.* B **92** 134405
[20] Lamago D, Georgii R, Pfleiderer C and Böni P 2006 *Physica* B **385-386** 385
[21] Pappas C, Lelievre-Berna E, Falus P, Bentley P M, Moskvin E, Grigoriev S, Fouquet P and Farago B 2009 *Phys. Rev. Lett.* **102** 197202
[22] Mühlbauer S, Binz B, Jonietz F, Pfleiderer C, Rosch A, Neubauer A, Georgii R and Böni P 2009 *Science* **323** 915
[23] Yu X Z, Onose Y, Kanazawa N, Park J H, Han J H, Matsui Y, Nagaosa N and Tokura Y 2010 *Nature* **465** 901
[24] Yu X Z, Kanazawa N, Onose Y, Kimoto K, Zhang W Z, Ishiwata S, Matsui Y and Tokura Y 2011 *Nat. Mater.* **10** 106
Yu X Z, Kanazawa N, Zhang W Z, Nagai T, Hara T, Kimoto K, Matsui Y, Onose Y and Tokura Y 2012 *Nat. Commun.* **3** 988
Tonomura A, Yu X, Yanagisawa K, Matsuda T, Onose Y, Kanazawa N, Park H S and Tokura Y 2012 *Nano Lett.* **12** 1673
[25] Wilson M N, Karhu E A, Quigley A S, Rößler U K, Butenko A B, Bogdanov A N, Robertson M D and Monchesky T L 2012 *Phys. Rev.* B **86** 144420
Yokouchi T, Kanazawa N, Tsukazaki A, Kozuka Y, Kikkawa A, Taguchi Y, Kawasaki M, Ichikawa M, Kagawa F and Tokura Y 2015 *J. Phys. Soc. Japan* **84** 104708
[26] Huang S X and Chien C L 2012 *Phys. Rev. Lett.* **108** 267201
[27] Heinze S, von Bergmann K, Menzel M, Brede J, Kubetzka A, Wiesendanger R, Bihlmayer G and Blügel S 2011 *Nat. Phys.* **7** 713
[28] Kézsmárki I *et al* 2015 *Nat. Mater.* **14** 1116–22
[29] Tokunaga Y, Zu X Z, White J S, Ronnow H M, Morikawa D, Taguchi Y and Tokura Y 2015 *Nat. Commun.* **6** 7638
[30] Seki S, Yu X Z, Ishiwata S and Tokura Y 2012 *Science* **336** 198
[31] Romming N, Hanneken C, Menzel M, Bickel J E, Wolter B, von Bergmann K, Kubetzka A and Wiesendanger R 2013 *Science* **341** 636
[32] Romming N, Kubetzka A, Hanneken C, von Bergmann K and Wiesendanger R 2015 *Phys. Rev. Lett.* **114** 177203
Marrows C H 2015 *Physics* **8** 40
[33] Bogdanov A and Hubert A 1994 *Phys. Stat. Sol.* (*b*) **186** 527
[34] Kiselev N S, Bogdanov A N, Schäfer R and Rößler U K 2011 *J. Phys. D: Appl. Phys.* **44** 392001
[35] Rybakov F N, Borisov A B and Bogdanov A N 2013 *Phys. Rev.* B **87** 094424
[36] Rybakov F N, Borisov A B, Blügel S and Kiselev N S 2015 *Phys. Rev. Lett.* **115** 117201
[37] Komineas S and Papanicolaou N 2015 *Phys. Rev.* B **92** 064412
[38] Hubert A and Schäfer R 1998 *Magnetic Domains* (Berlin: Springer)
[39] Tu Y 1971 *J. Appl. Phys.* **42** 5704
[40] Cape J A and Lehman G W 1971 *J. Appl. Phys.* **42** 1277
Bogdanov A N and Yablonskii D A 1980 *Sov. Phys. Solid State* **22** 399
[41] von Bergmann K, Menzel M, Kubetzka A and Wiesendanger R 2015 *Nano Lett.* **15** 3280
[42] Butenko A B, Leonov A A, Rößler U K and Bogdanov A N 2010 *Phys. Rev.* B **82** 052403
[43] Lin S Z, Reichhardt C, Batista C D and Saxena A 2013 *Phys. Rev.* B **87** 214419
[44] Rohart S and Thiaville A 2013 *Phys. Rev.* B **88** 184422
[45] Kim J-V, Garcia-Sanchez F, Sampaio J, Moreau-Luchaire C, Cros V and Fert A 2014 *Phys. Rev.* B **90** 064410
[46] Sampaio J, Cross V, Rohart S, Thiaville A and Fert A 2013 *Nat. Nanotech.* **8** 839
[47] Leonov A O, Rößler U K and Mostovoy M 2014 *EPJ: Web of Conf.* **75** 05002
[48] Butenko A B, Leonov A A, Bogdanov A N and Rößler U K 2009 *Phys. Rev.* B **80** 134410
[49] Iwasaki J, Mochizuki M and Nagaosa N 2013 *Nat. Nanotech.* **8** 742
[50] Zhang X, Zhao G P, Fangohr H, Liu J P, Xia W X and Morvan F J 2015 *Sci. Rep.* **5** 7643
[51] Nagaosa N and Tokura Y 2013 *Nat. Nanotech.* **8** 899
[52] Belavin A A and Polyakov A M 1975 *Sov. Phys. JETP Lett.* **22** 245
[53] Thiele A A 1970 *J. Appl. Phys.* **41** 1139
[54] Bran C, Butenko A B, Kiselev N S, Wolff U, Schultz L, Hellwig O, Rößler U K, Bogdanov A N and Neu V 2009 *Phys. Rev.* B **79** 024430
[55] Dupe B, Hoffmann M, Paillard C and Heinze S 2014 *Nat. Commun.* **5** 4030
[56] Meynell S A, Wilson M N, Fritzsche H, Bogdanov A N and Monchesky T L 2014 *Phys. Rev.* B **90** 014406
Wilson M N, Karhu E A, Lake D P, Quigley A S, Bogdanov A N, Rößler U K and Monchesky T L 2013 *Phys. Rev.* B **88** 214420
[57] Hagemeister J, Romming N, von Bergmann K, Vedmedenko E Y and Wiesendanger R 2015 *Nat. Commun.* **6** 8455
[58] Leonov A O, Dragunov I E, Rößler U K and Bogdanov A N 2014 *Phys. Rev.* E **90** 042504
[59] Ackerman P J, Trivedi R P, Senyuk B, van de Lagemaat J and Smalyukh I I 2014 *Phys. Rev.* E **90** 012505
[60] Wright G H and Mermin N D 1989 *Rev. Mod. Phys.* **61** 385
[61] Bak P and Jensen M H 1980 *J. Phys. C: Solid State Phys.* **13** L881
[62] Bogdanov A N, Rößler U K and Pfleiderer C 2005 *Physica* B **359-61** 1162
[63] Abrikosov A A 1957 *Sov. Phys. JETP* **5** 1174
[64] de Gennes P G 1966 *Superconductivity of Metals and Alloys* (New York: W A Benjamin)
[65] Moreau-Luchaire C *et al* 2016 *Nat. Nanotech.* **11** 444–8
[66] Woo S *et al* 2016 *Nat. Mater.* **15** 501–6

[67] Jiang W et al 2015 Science 349 283
[68] Bogdanov A N and Yablonskii D A 1989 Sov. Phys. JETP 69 142
[69] Bogdanov A N, Rößler U K, Wolf M and Müller K H 2002 Phys. Rev. B 66 214410